Infection of Alfalfa Cotyledons by an Incompatible but Not a Compatible Species of Colletotrichum Induces Formation of Paramural Bodies and Secretion of EVs

Suchismita Ghosh, 10 Kamesh C. Regmi, 10 Barry Stein, 2 Jun Chen, 2 Richard J. O'Connell, 3 and Roger W. Innes^{1,†}

- ¹ Department of Biology, Indiana University Bloomington, Bloomington, IN 47405, U.S.A.
- ² Indiana University Bloomington Electron Microscopy Center, Indiana University Bloomington, Bloomington, IN 47405,
- ³ Université Paris-Saclay, UR BIOGER, INRAE, Palaiseau 91120, France

Accepted for publication 28 June 2024.

Hemibiotrophic fungi in the genus Colletotrichum employ a biotrophic phase to invade host epidermal cells followed by a necrotrophic phase to spread through neighboring mesophyll and epidermal cells. We used serial block face-scanning electron microscopy (SBF-SEM) to compare subcellular changes that occur in Medicago sativa (alfalfa) cotyledons during infection by Colletotrichum destructivum (compatible on M. sativa) and C. higginsianum (incompatible on M. sativa). Three-dimensional reconstruction of serial images revealed that alfalfa epidermal cells infected with C. destructivum undergo massive cytological changes during the first 60 h following inoculation to accommodate extensive intracellular hyphal growth. Conversely, inoculation with the incompatible species C. higginsianum resulted in no successful penetration events and frequent formation of papillalike structures and cytoplasmic aggregates beneath attempted fungal penetration sites. Further analysis of the incompatible interaction using focused ion beam-scanning electron microscopy (FIB-SEM) revealed the formation of large multivesicular bodylike structures that appeared spherical and were not visible in compatible interactions. These structures often fused with the host plasma membrane, giving rise to paramural bodies that appeared to be releasing extracellular vesicles (EVs). Isolation of EVs from the apoplastic space of alfalfa leaves at 60 h postinoculation showed significantly more vesicles secreted from alfalfa

[†]Corresponding author: R. W. Innes; rinnes@indiana.edu

Current address for K. C. Regmi: Department of Biology, Kenyon College, Gambier, OH 43022, U.S.A.

Funding: This research was funded by the United States National Science Foundation Division of Integrative Organismal Systems Plant Biotic Interactions and Plant Genome Research programs (award numbers IOS-1645745, IOS-1842685, and IOS-2141969). S. Ghosh was supported by a Carlos Miller fellowship from the Indiana University Foundation. The INRAE BIOGER unit was supported by Saclay Plant Sciences-SPS (ANR-17-EUR-0007). The Thermo Fisher Teneo VolumeScope used was funded by an equipment grant from the National Institutes of Health (grant number 1S10OD023501).

e-Xtra: Supplementary material is available online.

The author(s) declare no conflict of interest.

Copyright © 2024 The Author(s). This is an open and distributed under the CC BY-NC-ND 4.0 International license. Copyright © 2024 The Author(s). This is an open access article infected with incompatible fungus compared with compatible fungus, which in turn was more than produced by noninfected plants. Thus, the increased frequency of paramural bodies during incompatible interactions correlated with an increase in EV quantity in apoplastic wash fluids. Together, these results suggest that EVs and paramural bodies contribute to immunity during pathogen attack in alfalfa.

Keywords: Colletotrichum destructivum, Colletotrichum higginsianum, extracellular vesicles, focused ion beam-scanning electron microscopy (FIB-SEM), IMOD, Medicago sativa, multivesicular bodies (MVB), paramural bodies, serial block face-scanning electron microscopy (SBF-SEM), three-dimensional-electron microscopy (3D-EM)

The Colletotrichum genus of fungal pathogens, which contains 280 accepted species, attacks over 3,200 species of dicot and monocot species worldwide (Bhunjun et al. 2021; Crous et al. 2004; Liu et al. 2022; O'Connell et al. 2012; Yan et al. 2018). Colletotrichum infects many important food crops, causing anthracnose leaf spot disease, which can cause large reductions in yield. Well-studied Colletotrichum-host interactions include C. lindemuthianum-bean (O'Connell et al. 1985), C. graminicola-maize (Mims and Vaillancourt 2002; O'Connell et al. 2012), C. higginsianum-Arabidopsis (O'Connell et al. 2004), C. sublineola-sorghum (Wharton et al. 2001), C. orbiculare-cucumber (Xuei et al. 1988), and C. destructivumalfalfa (Damm et al. 2014; Latunde-Dada et al. 1997). Of these, the infection of Arabidopsis by C. higginsianum is considered a model because both plant and fungal partners can be genetically manipulated (O'Connell et al. 2004; Yan et al. 2018).

Colletotrichum begins its infection process by forming a melanized globular structure called the appressorium that arises from germ tubes produced by asexual fungal spores (conidia). Appressoria attach to leaf epidermal cells and form penetration pegs, allowing the fungus to push through epidermal cell walls, after which they form biotrophic hyphae that invaginate the host cell plasma membrane without rupturing it (Latunde-Dada et al. 1997; Mims and Vaillancourt 2002; O'Connell 1987; Wharton et al. 2001). This biotrophic phase is transient, lasting only 2 to 3 days on average (O'Connell et al. 2012; Yan et al. 2018). This is followed by a necrotrophic phase, where hyphae invade neighboring cells, killing the plant (Heath 2000; Latunde-Dada et al.

1997). This biphasic mode of pathogenicity is called hemibiotrophy (Luttrell 1974).

C. higginsianum expresses a large number of genes encoding secreted proteins during infection of Arabidopsis, including enzymes that mediate degradation of plant cell wall components such as cellulose, hemicellulose, and pectin (O'Connell et al. 2012). Expression of these enzymes is especially high during appressorium formation, indicating that these enzymes contribute to the penetration of the epidermal cell wall. During establishment of the biotrophic phase, genes encoding secondary metabolism enzymes and various effector proteins are induced (Kleemann et al. 2012). During the switch to necrotrophy, C. higginsianum starts to produce a large array of proteases, carbohydrate-active enzymes, and other lytic enzymes, as well as membrane transporters (O'Connell et al. 2012). During the necrotrophic phase, genes encoding necrosis-inducing proteins and many degradative enzymes such as proteases and cell walldegrading enzymes are also up-regulated that cause tissue destruction and eventual cell death (Heath 2000; Latunde-Dada et al. 1997; O'Connell et al. 2012).

Ultrastructural studies using electron microscopy (EM) have shown that Colletotrichum species often induce formation of electron-opaque structures called cell wall appositions or "papillae" beneath attempted sites of appressorial penetration. These papillae contain callose, a β-1,3-glucan polymer (Jacobs et al. 2003; Mims and Vaillancourt 2002). Comparison of susceptible and resistant cultivars of French bean (Phaseolus vulgaris) infected with C. lindemuthianum showed that papillae formed beneath appressoria at similar frequencies in both cases, indicating that papilla formation is not specifically associated with unsuccessful penetration events (O'Connell et al. 1985). Similar studies between susceptible and resistant cultivars of Sorghum bicolor infected with C. sublineola also revealed formation of papillae in both susceptible and resistant cultivars; however, the papillae formed in the resistant cultivar were more electronopaque compared with the susceptible cultivar, suggesting deposition of additional materials in the resistant cultivar (Wharton et al. 2001). In both studies, infection of the susceptible cultivar began with the formation of an infection vesicle that arose from the appressorium and formed inside the host epidermal cell, giving rise to a primary biotrophic hypha. In the resistant cultivar, however, fewer infection vesicles were observed, and formation of biotrophic hyphae was rare (O'Connell et al. 1985; Wharton et al. 2001).

The above studies focused on comparison of resistant and susceptible cultivars being infected by the same fungal strain. It is also informative to compare responses in a single host variety to infection by 'compatible' (adapted) and 'incompatible' (nonadapted) species of Colletotrichum. In this context, incompatible interactions are defined as interactions between a given fungal species that cannot infect any varieties of a given plant species (Heath 2000). For example, C. graminicola, which normally infects maize, cannot infect any varieties of Arabidopsis and is thus considered incompatible on Arabidopsis, whereas C. higginsianum can infect most accessions of Arabidopsis and is thus considered compatible on Arabidopsis (O'Connell et al. 2004; Shimada et al. 2006; Yan et al. 2018). Comparison of Arabidopsis infected with C. higginsianum to Arabidopsis infected with incompatible Colletotrichum species has shown that papillae were smaller in the compatible interaction and formed with lower frequency compared with the incompatible species (Shimada et al. 2006). Differences between compatible and incompatible responses were likewise reported in oats infected with C. graminicola (nonadapted) versus infection of maize with the same fungal strain (adapted) (Politis 1976; Politis and Wheeler 1973), suggesting that papillae contribute to immunity.

Formation of papillae is often associated with the accumulation of multivesicular endosomes adjacent to the papillae (An et al. 2006b). These endosomes are typically approximately 1 μ m in diameter and contain multiple intraluminal vesicles of variable size. These endosomes are often referred to as multivesicular bodies (MVBs), but it should be noted that their appearance differs from that of MVBs associated with transport of plasma membrane receptors to lysosomes or vacuoles, which typically are less than 0.5 μ m in diameter and contain smaller intraluminal vesicles with greater electron density and less variation in size (Buono et al. 2016). Multivesicular endosomes adjacent to papillae sometimes appear to fuse with the plasma membrane, at which point they are called paramural bodies (PMBs) (Marchant and Robards 1968).

In this study, we used *Medicago sativa* (alfalfa) to compare subcellular responses to infection by compatible (*C. destructivum*) and incompatible (*C. higginsianum*) fungal species. These two species are phylogenetically very close, belonging to the same phylogenetic clade called the Destructivum species complex (Damm et al. 2014). All the members of this species complex share the same infection process, where the biotrophic hyphae are confined to one epidermal cell. In contrast, the biotrophic hyphae of most other hemibiotrophic *Colletotrichum* species extend into many host cells, including the mesophyll (da Silva et al. 2020; Damm et al. 2014). Examples include *C. lindemuthianum* and *C. orbiculare*, which belong to the Orbiculare species complex, and *C. sublineola* and *C. graminicola*, which belong to the Graminicola species complex (Bhunjun et al. 2021; Weir et al. 2012).

Alfalfa is commonly infected by *C. destructivum* (Damm et al. 2014; Latunde-Dada et al. 1997), which causes anthracnose disease in many forage and grain legume species including clover, alfalfa, cowpea, and lentil (Damm et al. 2014). *C. higginsianum*, which infects many crucifer species, including *Arabidopsis*, does not infect alfalfa. In this study, we wished to assess whether compatible and incompatible interactions in this system differed with regards to papilla formation and production of PMBs.

To assess papilla formation and PMBs, we performed threedimensional (3D) EM using both serial block face-scanning electron microscopy (SBF-SEM) and focused ion beam-scanning electron microscopy (FIB-SEM). All prior EM-based studies of plant-Colletotrichum interactions have used standard transmission electron microscopy (TEM), which provides twodimensional (2D) cross-sections of infected cells (Kleemann et al. 2012; Mims and Vaillancourt 2002; O'Connell et al. 1985; Wharton et al. 2001). The 2D nature of these micrographs prevents complete understanding of the nature of infection structures observed. In contrast, SBF-SEM and FIB-SEM enable generation of 3D images by producing hundreds of serial sections in an automated manner, which can then be computationally assembled into a 3D structure (Denk and Horstmann 2004; Xu et al. 2017). SBF-SEM and FIB-SEM differ from each other in the way that the serial sections are generated. The former uses a microtome housed inside the SEM to remove approximately 40-nm sections from the sample block, with the fresh face imaged after removal of each section. FIB-SEM, in contrast, uses an ion beam to remove a 5- to 10-nm layer from the sample block between images. FIB-SEM imaging thus provides a higher resolution in the z dimension. Both SBF-SEM and FIB-SEM reveal details such as the 3D shape and volume of the fungal hyphae, the topological nature of the circular objects observed in a single micrograph (e.g., spheres versus tubes), and the extent of membrane degradation throughout the volume of an infected plant cell, none of which are possible to assess from a single ultrathin section in classical TEM.

Using SBF-SEM and FIB-SEM, we were able to generate 3D models of the plant-fungal interface in both compatible and in-

compatible interactions. From these models, we obtained several important insights. At 24 h postinoculation (hpi), both compatible and incompatible interactions displayed formation of fungal appressoria and induction of cytoplasmic vesicles and tubules around the periphery of the epidermal cell, with a higher concentration adjacent to appressoria. Neither interaction showed penetration of the plant cell wall by the fungus at this time point, and ultrastructural differences between the two interactions appeared minor. At 60 hpi, in contrast, the differences were large. In the compatible interaction, biotrophic hyphae had largely displaced the central vacuole of epidermal cells, which requires a massive increase in host cell plasma membrane to accommodate these hyphae. While cytoplasmic vesicles and tubules were still abundant in the plant cell cytoplasm, no obvious papillae or PMBs were visible in the compatible interaction. In the incompatible interaction, no biotrophic hyphae or penetration pegs had formed despite abundant appressoria being present. Notably, large cytoplasmic aggregates had formed underneath many appressoria, which we think are precursors of papillae, and numerous PMBs were observed spread around the periphery of epidermal cells. We also detected an increase in extracellular vesicle (EV) number in apoplastic wash fluids, which is consistent with the increase in PMBs. Together, these observations support the assumption that papillae and EVs contribute to nonhost resistance in Medicago.

Results

Both compatible and incompatible fungal species induce vesicle formation in host epidermal cells prior to penetration

We wanted to understand whether the infection of alfalfa with its compatible *Colletotrichum* species induces visible changes in host cell ultrastructure prior to the formation of biotrophic hyphae. We therefore chose 24 hpi to visualize these subcellular changes, as we never observed biotrophic hyphae at this time point.

To image subcellular structures, we used SBF-SEM and chemical fixation of samples. We employed chemical fixation rather than high-pressure freezing to preserve appressoria. In prior SBF-SEM analyses of *Arabidopsis* cotyledons infected with C. higginsianum (a compatible interaction), we observed that appressoria were entirely missing despite the presence of abundant intracellular hyphae (Regmi et al. 2024). In this study, we wished to capture subcellular defense responses in incompatible interactions that lacked intracellular hyphae, so we needed to be able to locate sites of attempted penetration. This proved impossible with high-pressure freezing, hence our decision to employ chemical fixation instead, despite the advantages of high-pressure freezing for preserving membrane ultrastructure. A limitation of chemical fixation is that dehydration of cells during the fixation process can lead to changes in membrane structures. In our analyses below, we therefore focused on membrane structures that were absent in our noninfected controls and, when comparing compatible and incompatible interactions, structures that were unique to one or the other.

For the mock inoculation, 200 serial images were obtained (Fig. 1A; Supplementary Video S1), and for the compatible infection (*C. destructivum*), 201 serial images were obtained (Fig. 1B to F; Supplementary Video S2). For both samples, this represents approximately 8 µm of cell depth. The mock-infected alfalfa cotyledon (Fig. 1A) showed an intact plant cell membrane as well as an intact tonoplast with very little intracellular vesiculation (enlarged in Fig. 1A1). In contrast, the *C. destructivum*-infected cotyledon displayed abundant intracellular vesiculation (Fig. 1B). As expected, no appressoria were present in the mock-infected sample (Fig. 1A), whereas dome-shaped appressoria

were concentrated over anticlinal cell walls in the valleys between epidermal cells of the infected cotyledon (Fig. 1B). This is expected because spores tend to accumulate in this location, so appressoria form there as a result. Electron-opaque vesicular structures were visible that appeared to be near the vicinity of the plant cell plasma membrane. These structures could be grouped into two classes based on their level of staining: heavily stained (electron-opaque; yellow arrowheads) and lightly stained (blue arrowheads) (Fig. 1B and C). These electron-opaque circular structures were absent from mock-inoculated plant cells as seen in Figure 1A and Supplementary Video S1.

To assess the 3D shape of the vesicle-like structures, we used the free software program IMOD (Kremer et al. 1996). Figure 1D shows a representative grayscale image with the model superimposed on top of it, which is 180 degrees rotated from Figure 1B and C. The entire model is shown rotating in space in Supplementary Video S3; 3D imaging is required to distinguish between spherical and tubular structures that both appear as circles in 2D sections. We modeled the circular structures shown in Figure 1B and C, maintaining the same color code. Figure 1E is a snapshot of the model that reveals that even though these structures appeared vesicular in a 2D SEM image, some of them are in fact tubular rather than spherical, and in this snapshot, these tubular structures are roughly in the same orientation. Figure 1F shows the model rotated to better visualize their tubular nature. The electron-opaque structures (yellow) were more abundant than the less densely stained structures (blue). Both classes of structures appeared near the plasma membrane, suggesting that they may be a response to the fungal appressoria. Some of these structures were vesicular, as seen by their spherical shape, while some taper into tubes along the periphery of the plant cell under attack. Supplementary Figure S1B shows a single frame from an SBF-SEM image stack of a second compatible infection at 24 hpi, while Supplementary Video S4 shows the full set of images. These images show the same pattern of vesiculation as observed in Supplementary Video S2.

Next, we examined the response of alfalfa to inoculation with an incompatible fungal species (C. higginsianum) to assess whether the response differs from a compatible strain at 24 h. We collected 251 serial images, representing approximately 10 µm of cell depth (Fig. 2; Supplementary Video S5). Figure 2A shows the 111th image of the image stack, while Figure 2B shows the 212th image. Like its compatible counterpart (Fig. 1), we observed both electron-opaque and less-dense vesicular structures (Fig. 2A and B; yellow and blue arrows). This indicates that the intracellular vesiculation observed in the compatible interaction also occurs during an incompatible interaction. In addition to the electron-opaque and less-dense vesicular structures, we observed a third type of circular structure that was more prominent in the incompatible interaction, which appeared to be membrane-bound circles with no visible internal staining (indicated by pink arrows in Fig. 2A). These structures were rarely observed in compatible interactions.

Figure 2C shows a snapshot of a 3D model generated from the entire image stack of the incompatible interaction. Supplementary Video S6 shows the full model. Figure 2D and E are snapshots of the model rotated vertically at 90 and 180 degrees, respectively, to reveal the nature of the electron-opaque and less-dense structures. Similar to the compatible interaction at 24 h, penetration of plant cells by fungal hyphae was not observed, although numerous appressoria were present on the cell surface. Some of the electron-opaque structures formed a meshwork of tubules similar to that observed in the compatible interaction (yellow in the model). The lighter-stained structures (blue) appeared to be more vesicular. The hollow-looking pink structures appeared to form both spherical and tubular structures. Supplementary Figure S1C and Supplementary Video S7 show a second

incompatible inoculation of alfalfa imaged at 24 h, revealing a similar pattern of vesiculation as observed in Supplementary Video S5.

Supplementary Figure S2A quantifies the number of vesicles and tubules observed in either compatible or incompatible interactions at 24 h for both the electron opaque (yellow) and the lightly stained (blue) structures across 20 µm of plant cell depth. Since the very lightly stained hollow structures (pink) were rarely visible or were too small to model in the compatible interaction, we did not quantify those particles. The 3D model was used to distinguish between the vesicles and the tubules. For our calculations, any structure that was twice as long as it was wide was considered a tubule. Both the compatible interaction

(Supplementary Videos S2 and S4) and incompatible interaction (Supplementary Videos S6 and S7) were modeled and quantified for the graph. These analyses did not show any significant differences between the number of vesicles and tubules observed between the compatible and incompatible interactions. The electron opaque particles (yellow) seemed to form more tubules than vesicles, whereas the lightly stained particles (blue) formed more vesicles than tubules in both interaction types at 24 h.

C. destructivum biotrophic hyphae displace the central vacuoles of epidermal cells by 60 hpi

The above analyses revealed cellular responses occurring prior to formation of biotrophic hyphae but did not reveal large

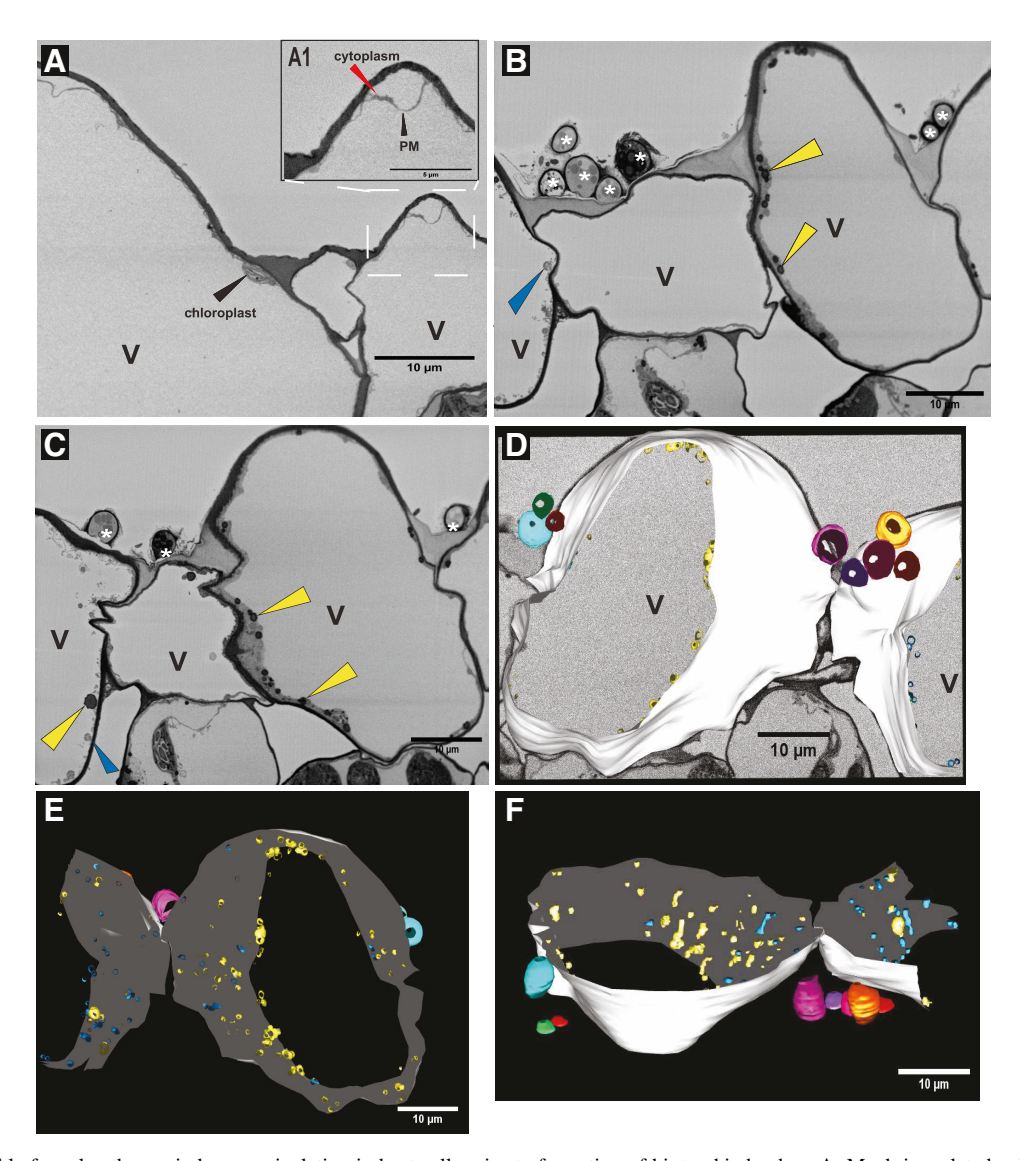


Fig. 1. A compatible fungal pathogen induces vesiculation in host cells prior to formation of biotrophic hyphae. A, Mock-inoculated epidermal cells show very little vesiculation. The image shows the first micrograph from a stack of 200 serial block face-scanning electron microscopy (SBF-SEM) images of three epidermal cells on an alfalfa cotyledon mock-inoculated with water and imaged 60 h postinoculation (hpi). Supplementary Video S1 shows all 200 images in this stack. Note large central vacuoles (V) and the chloroplast visible in the epidermal cell. A1, Enlarged boxed region that shows the plasma membrane (PM) and thin peripheral cytoplasm. *Colletotrichum destructivum* induces vesiculation by 24 hpi; panels show the B, 14th and C, 84th micrograph from an SBF-SEM image stack of alfalfa epidermal cells infected with *C. destructivum* (a compatible species) and imaged 24 hpi. Fungal appressoria are marked with an asterisk (*) and appear as dome-shaped structures on the adaxial surface of host epidermal cells. Heavily stained circular structures are indicated by yellow arrows. These structures appear mostly along the PM of the plant cell and are absent from mock-infected cotyledons (A). Blue arrows indicate moderately stained circular structures. Supplementary Video S2 shows all 201 images in this stack. D, Three-dimensional model of two adjacent epidermal cells superimposed on a grayscale SBF-SEM image from the same stack shown in B and C. This model was generated using IMOD software. The plant cell wall is shown in white for the two adjacent cells. Fungal appressoria are shown as colored donut-shaped structures sitting above the plant cell. Heavily stained vesiculo-tubular structures observed in images B and C are modeled in yellow, while moderately stained structures are modeled in blue. E, Three-dimensional model of image stack; F, the same model rotated 90 degrees vertically. Please refer to Supplementary Video S3 to see this model rotating in space.

differences between compatible and incompatible interactions. We therefore imaged infection sites at 60 hpi. At this time point, we expected to see extensive biotrophic hyphae in the compatible interaction but very little cell death. In incompatible interactions, in contrast, we expected to see a lack of biotrophic hyphae and possibly the death of epidermal cells and/or formation of defensive structures such as papillae (cell wall appositions).

As seen in Figure 3, by 60 hpi, C. destructivum had extensively colonized the epidermal cell with its biotrophic hyphae, which largely displaced the central vacuoles of infected epidermal cells, although the plasma membrane and tonoplast remained intact. We were able to observe a penetration peg (black arrow in Fig. 3A), which is the site where the fungus penetrates the plant cell wall beneath the appressorium. This event could be captured because we imaged approximately 16 µm of the plant cell volume (398 sections) using the SBF-SEM (Supplementary Video S8), enabling us to find the rare section that captured such an event. We used IMOD to reconstruct the imaging volume in 3D, which allowed us to visualize the 3D branching structures of individual hyphae. We could not visualize any interfacial matrix at this resolution (material surrounding biotrophic hyphae that is expected to accumulate between the plasma membranes of the fungus and the plant). The biotrophic hyphae were highly stained. Intense fragmentation of the plant vacuolar membrane was seen in the vicinity of the biotrophic hyphae, as well as near the surface of the plant cell (Fig. 3A1). In contrast, the plant chloroplasts, mitochondria, and plasma membrane remained intact, indicating that the fungus was still in its biotrophic phase. Figure 3B represents the 300th micrograph from the same image stack, which shows the biotrophic hyphae almost displacing the entire volume of the plant vacuole, with the vacuole becoming highly fragmented (Fig. 3B1). Like the 24-h time point, densely stained structures were also observed (indicated with yellow arrows in Fig. 3B1 and modeled using the same color code). A 3D model of the entire imaging volume was first created without the vacuo-

lar membrane to simplify the model (Supplementary Video S9). Next, we modeled the area of vacuolar membrane disintegration as mentioned above, which can be seen in Supplementary Video S10. Figure 3C shows a snapshot of the model with the biotrophic hyphae, the heavily stained yellow structures, and the hollow structures in pink. For ease of visualization, biotrophic hyphae 3 and 4 are dotted to better see the yellow and pink structures along the periphery of the membrane. Figure 3D represents a grayscale image superimposed on the model, which enabled us to connect the biotrophic hyphae as continuous structures occupying nearly the entire plant cell volume. Figure 3E is a 90degree rotated image of the same model shown in Figure 3D. To capture the amount of membrane disintegration, the same model is rotated and shown in Figure 3F, showing the extensive nature of these structures, roughly in the same orientation much like Figure 1F. The heavier-stained yellow structures appear more tubular and seem to form an interconnected mesh near the plant cell wall. The lighter-stained structures are occasionally vesicular spheres but are mostly tubular; however, they seem to be less interconnected compared with the yellow ones. Overall, the fungus occupied the majority of the plant cell, suggesting massive expansion of the plant plasma and tonoplast membranes must occur to accommodate the very large biotrophic hyphae. Supplementary Figure S1D shows a second compatible infection of alfalfa imaged at 60 hpi, while Supplementary Video S11 shows the entire SBF-SEM image stack. These images confirm the extensive remodeling of the host cell vacuolar and plasma membranes during the compatible interaction.

Given the extensive membrane remodeling and vesiculation observed by SBF-SEM, we wished to determine whether cell death was occurring during the compatible interaction. We thus stained cotyledons with trypan blue (Fernández-Bautista et al. 2016; O'Connell et al. 2004) at both 24 and 60 hpi. We observed no evidence of cell death at either time point with the compatible strain *C. destructivum* (Supplementary Fig. S3), even though

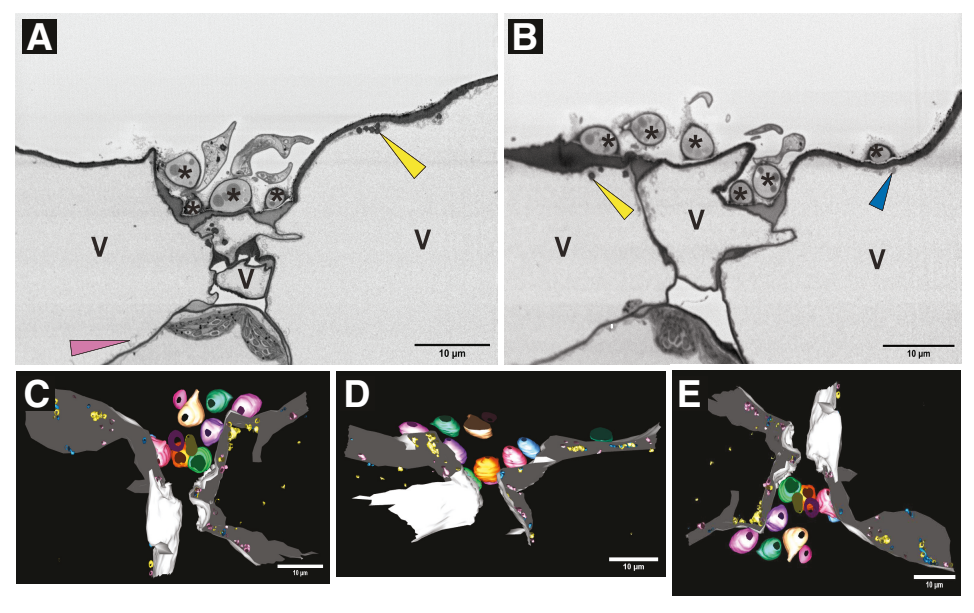


Fig. 2. An incompatible fungal pathogen induces vesiculation in host cells, including a third class of vesicles not observed during a compatible interaction. A and B, The 111th and 212th micrographs from a serial block face-scanning electron microscopy (SBF-SEM) image stack containing 251 images showing alfalfa epidermal cells infected with *Colletotrichum higginsianum* (incompatible on alfalfa) and imaged at 24 h postinoculation (hpi). Very lightly stained circular structures, which were not observed in the compatible interaction, are seen throughout the entire stack of 251 images and are marked with pink arrowheads. Heavily stained circular structures are indicated by yellow arrowheads, while moderately stained structures are indicated by blue arrowheads. Supplementary Video S5 shows all 251 images in this stack. C, Three-dimensional (3D) model of the entire volume of 251 SBF-SEM images. Supplementary Video S6 shows this 3D model rotating in space; D and E, the same model rotated 90 and 180 degrees vertically to better visualize the vesiculo-tubular structures. Heavily stained structures are modeled in yellow, moderately stained structures are modeled in blue, and lighter-stained structures are modeled in pink. V = vacuole; * appressorium.

this interaction is expected to switch to a necrotic phase by 72 hpi.

The incompatible fungus *C. higginsianum* fails to penetrate alfalfa epidermal cells

Attempted penetration of plant epidermal cells by nonadapted fungal species often induces formation of localized defense structures known as cell wall appositions or papillae (An et al. 2006a, b; Rubiato et al. 2022). Extensive studies of barley infected with incompatible species of powdery mildew fungi have revealed formation of papillae or encasements as pre- and postinvasive defense structures, respectively (Assaad et al. 2004; Böhlenius et al. 2010; Heitefuss and Ebrahim-Nesbat 1986; Zeyen and Bushnel 1979). The incompatible interaction interface in the hemibiotrophic fungus *Colletotrichum* is less studied. We imaged incompatible interactions at the 60-h time point to

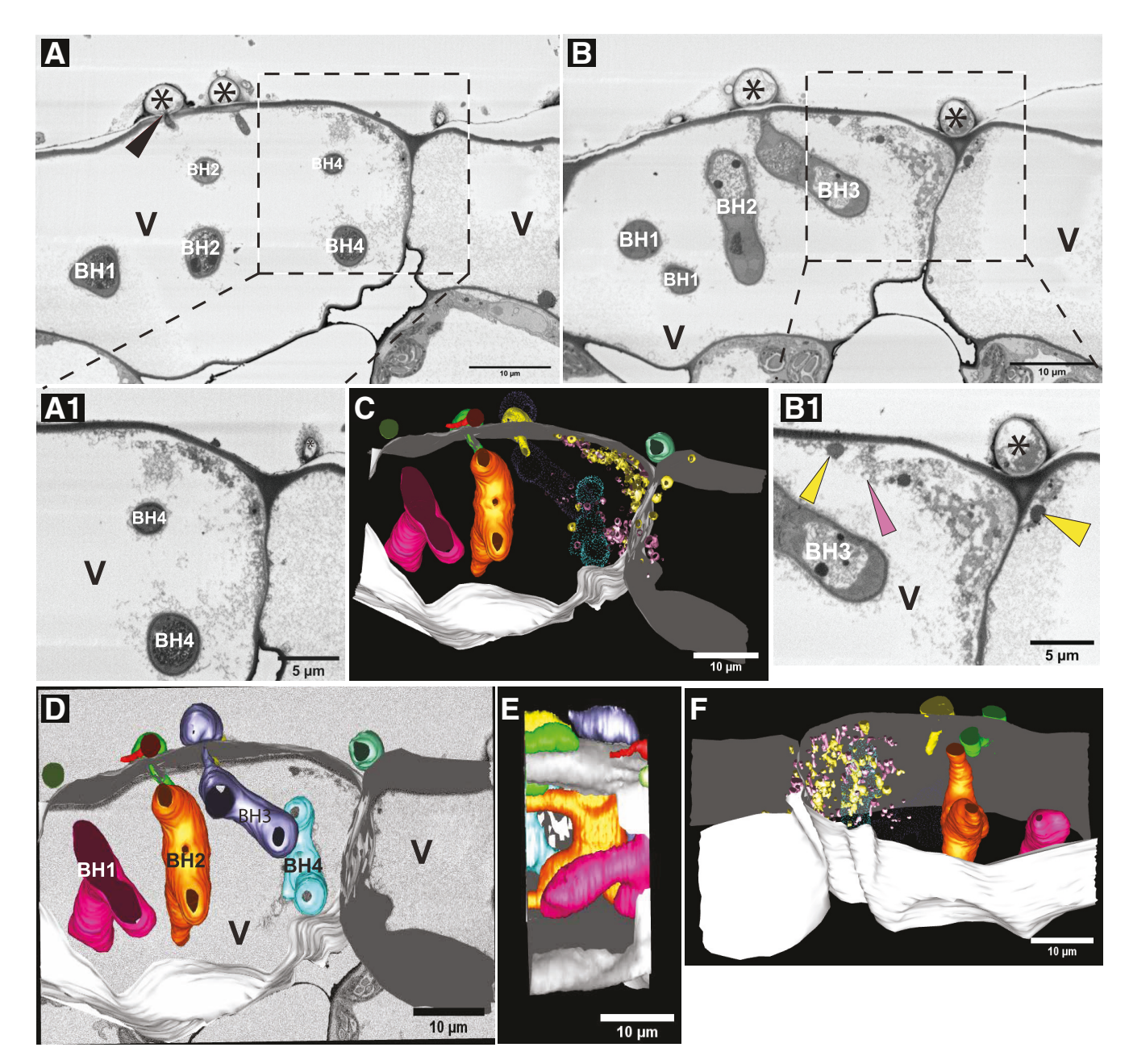


Fig. 3. Alfalfa cotyledons accommodate extensive biotrophic hyphae at 60 h postinoculation (hpi) with *Colletotrichum destructivum*; A and B, 100th and 300th micrograph, respectively, from a serial block face-scanning electron microscopy (SBF-SEM) image stack containing 398 images. A1 and B1, Enlarged boxed regions from panels A and B, respectively. The black arrowhead in panel A marks a fungal penetration peg. Biotrophic hyphae (BH) are numbered and correspond to the BH modeled in panel D. Heavily stained circular structures are indicated with yellow arrowheads in panel B1. These structures appear mostly along the plasma membrane of the plant cell. The pink arrowhead in B1 indicates lighter-stained circular structures. Supplementary Video S8 shows all 398 images in this stack. C, Three-dimensional model generated from this stack using IMOD. The plant cell wall is shown in white for the two adjacent cells. Note the extensive BH and vesiculo-tubular structures. The dark structures are modeled in yellow, while the lighter ones are modeled in pink. For the ease of visualization, BH3 and BH4 are dotted to better see the vesiculo-tubular structures near the plant plasma membrane. D, Three-dimensional model superimposed on a grayscale SBF-SEM image from the same stack. The BH are numbered 1 to 4 and correspond to those labelled in panels A and B. Supplementary Video S9 shows this model rotating in space; E, 90-degree rotation of the three-dimensional model showing the extensive hyphae extending across the depth of the epidermal cell; F, the same model shown in C rotated vertically to better visualize the vesiculo-tubular structures. Supplementary Video S10 shows a three-dimensional model of these structures. V = vacuole; * = appressorium.

compare the differences in host cell responses between compatible and incompatible *Colletotrichum* species.

Contrary to *C. destructivum* (compatible) (Fig. 3), *C. higginsianum* (incompatible) was unable to penetrate alfalfa epidermal cells even at 60 hpi (Fig. 4). Interestingly, as seen in Figure 4A and Supplementary Video S12, extensive aggregations of electron-opaque vesicles were observed near fungal appressoria. These electron-opaque vesicles may be local accumulations of cytoplasm or cytoplasmic aggregates that usually accompany the papilla response (Schmelzer 2002). These cytoplasmic aggregate-like structures were composed of three types of circular structures similar to those described in Figure 2 (densely stained, lightly stained, and hollow). In addition, we observed numerous circular membrane-bound structures that appeared to be fusing with the plant plasma membrane (red arrows in Fig. 4A1). These were not observed in the compatible inter-

action. Figure 4B shows the 500th micrograph, where we see another region of local accumulation of plant cytoplasm, which may also be a precursor of papilla deposition (red box). The red arrow again indicates a membrane-bound circular structure appearing to fuse with the plasma membrane. A top view image of the model is shown in Figure 4C, where the extensive interconnected network of papilla-likes structures along the host cell wall is clear. Figure 4D represents a snapshot of the model (Supplementary Video S13) that shows focused deposition of membrane material and reveals a highly interconnected mesh of vesiculo-tubular structures. The appressoria failed to form penetration pegs, and no biotrophic hyphae were observed inside host cells. Together, these results indicate that when alfalfa is infected with an incompatible Colletotrichum species, the fungus fails to penetrate the plant cell, while the plant cell creates an extensive interconnected network of vesiculo-tubular structures un-

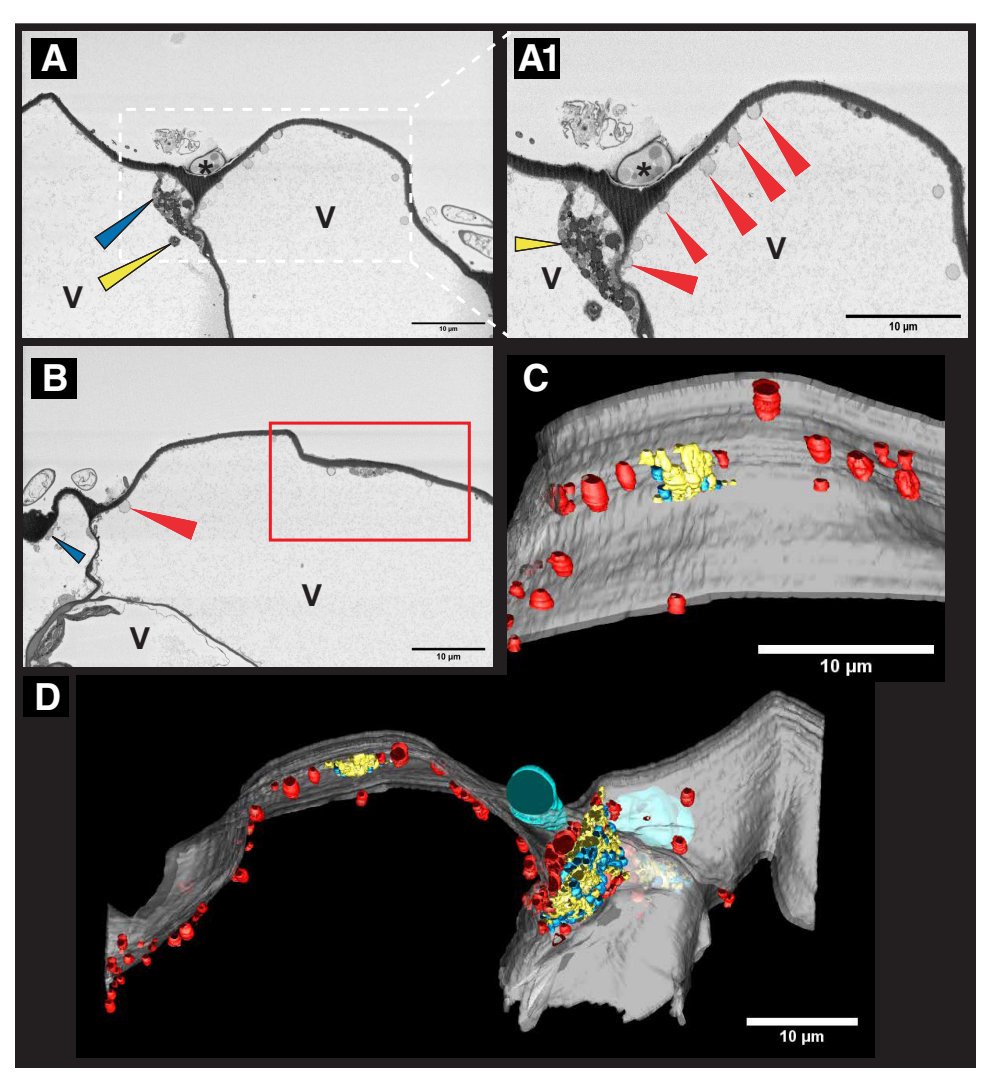


Fig. 4. Inoculation with an incompatible pathogen (*Colletotrichum higginsianum*) induces formation of paramural bodies in alfalfa epidermal cells. **A**, The first micrograph from a serial block face-scanning electron microscopy (SBF-SEM) image stack contains 500 images showing alfalfa epidermal cells infected with *C. higginsianum* and was imaged 60 h postinoculation (hpi). Supplementary Video S12 shows the entire 500-image stack and spans 20 μm of the plant cell. Heavily stained circular structures are marked with yellow arrowheads, and moderately stained structures are marked with blue arrowheads. **A1**, Enlarged boxed region from panel A, which shows lightly stained circles that appear to be fusing to the plant plasma membrane (red arrowheads). **B**, The 500th micrograph from the same image stack. The red arrowhead depicts a circular membrane-bound structure that appears to be fusing with the plasma membrane of the host. The red box shows another area of heavily stained structures similar to those shown in panel A1. **C**, Three-dimensional model of the region boxed in red in panel B viewed from the top. **D**, Three-dimensional model based on all 500 images made using IMOD. Two adjacent plant cell walls are shown in gray. An appressorium is shown in cyan, but no penetration pegs or biotrophic hyphae were observed in any of the 500 images, indicating that the fungus failed to penetrate the host cells. The circular-looking vesiculo-tubular structures are modeled in yellow (heavily stained), blue (moderately stained), and red (lightly stained structures that appear to be fusing with the plasma membrane). Supplementary Video S13 shows this model rotating in space. V = vacuole; * = appressorium.

derneath attempted fungal penetration sites. Furthermore, large membrane-bound vesicles form all along the periphery of the cell that appear to be fusing with the plasma membrane.

To assess whether the cellular changes induced by *C. higginsianum* were associated with a hypersensitive response (HR), we stained cotyledons with trypan blue to detect dead cells. We observed no cell death at either 24 or 60 hpi (Supplementary Fig. S3), indicating that resistance is not mediated by HR cell death in this interaction, possibly because the infection is stopped prior to formation of biotrophic hyphae, hence preventing translocation of effector proteins into host cells. We observed increased staining of cell walls with trypan blue (Supplementary Fig. S3), which is consistent with the failure to form penetration pegs and may reflect increased lignification associated with induction of cell wall-mediated defense responses.

To further assess changes in cell wall structure associated with attempted penetration events, we stained cotyledons with aniline blue, which binds to callose, a polysaccharide that accumulates in papillae that is thought to help block penetration of fungal hyphae (Ellinger et al. 2013; Luna et al. 2011). We observed large fluorescent puncta indicative of callose deposition, which were larger and more abundant in incompatible interactions compared with compatible interactions in both cotyledon and leaves (Supplementary Fig. S4). These results are consistent with the numerous papilla-like structures observed in SBF-SEM images.

The incompatible fungus *C. higginsianum* induces formation of PMBs

The membrane-bound vesicles that appeared to be fusing with the plasma membrane shown in Figure 4 appear similar to pre-

viously described PMBs (Marchant and Robards 1968), which form when MVBs fuse with the plasma membrane. To assess this more carefully, we enlarged a region of the plasma membrane that displayed an abundance of these structures (Fig. 5; Supplementary Video S14). Red arrows indicate putative PMBs. These seem to be a unique feature of the incompatible interaction, as we did not observe any such structures in the compatible interaction or mock-infected sample, suggesting that these structures are associated with immunity. Transmission electron micrographs of incompatible interactions of barley and Arabidopsis infected with biotrophic powdery mildew fungi have shown multivesicular endosomes and PMBs near attempted penetration sites (An et al. 2006b), which is consistent with this hypothesis, as have TEM images of broad bean plants infected with an incompatible cowpea rust fungus (Xu and Mendgen 1994). As shown in Figure 4, the PMBs observed in the incompatible interaction at 60 hpi are widely distributed along the cell periphery and are not specifically localized at attempted penetrated sites.

We quantified the number of PMBs observed across the 20 μ m of the plant cell imaged by SBF-SEM (Supplementary Fig. S2B). We also calculated the epidermal cell surface area imaged using the SBF-SEM image stack and Fiji software. For block 1 (Fig. 4; Supplementary Video S12), the surface area was approximately 1,746 μ m², and we counted 174 PMBs. For block 2 (Fig. 5; Supplementary Video S14), the surface area was approximately 1,478 μ m², and we counted 186 PMBs. The number of PMBs were comparable in the two blocks, although block 2 had more PMBs per unit of the cell surface area. To ensure that these PMBs were not an artifact of cell death, we stained infected

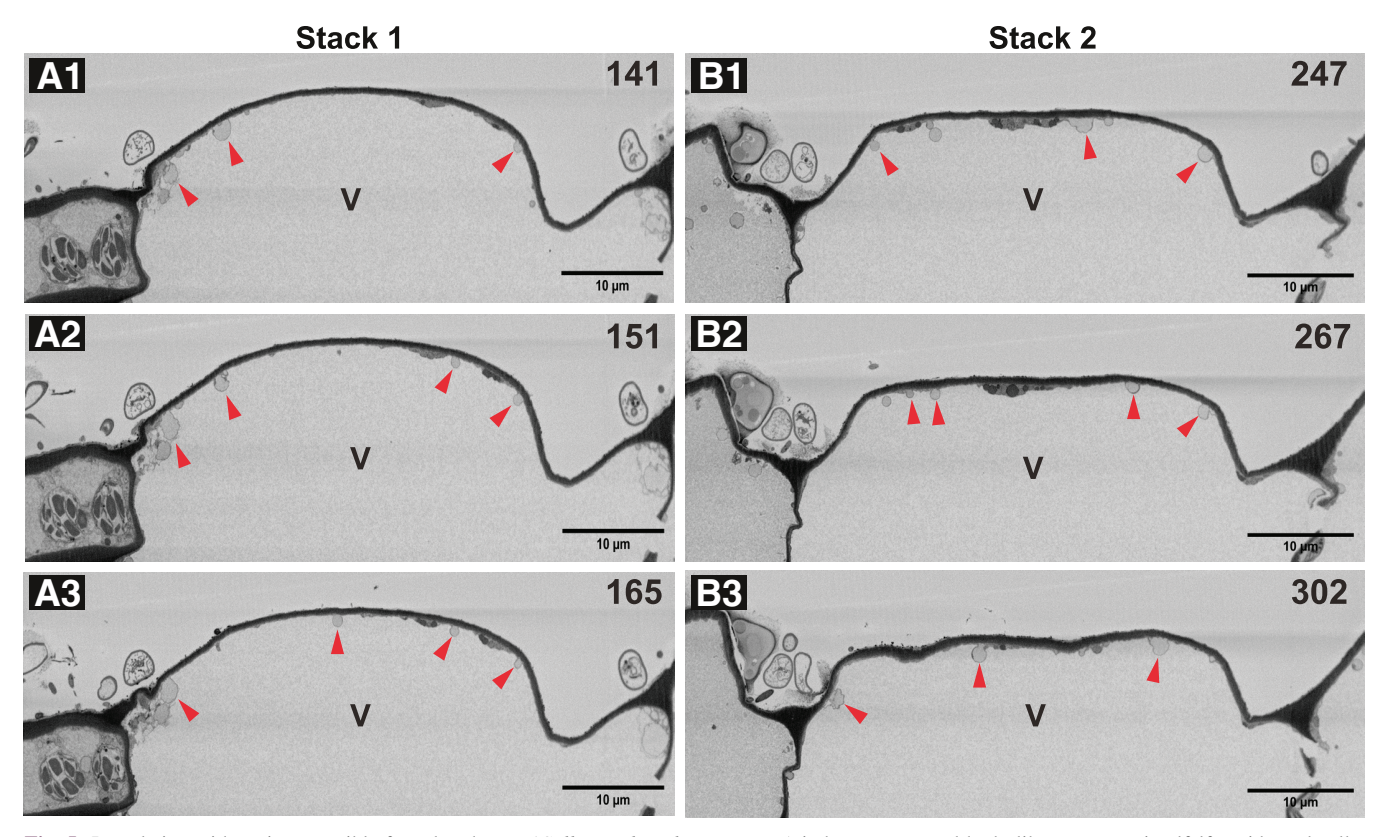


Fig. 5. Inoculation with an incompatible fungal pathogen (*Colletotrichum higginsianum*) induces paramural body-like structures in alfalfa epidermal cells. **A1, A2, and A3,** The 141st, 151st, and 165th micrographs from a serial block face-scanning electron microscopy (SBF-SEM) image stack containing 500 images showing alfalfa epidermal cells infected with *C. higginsianum* and imaged at 60 h postinoculation (hpi) (Event 1). **B1, B2, and B3,** The 247th, 267th, and 302nd micrographs from the same SBF-SEM image stack showing another event of paramural body fusion to the plasma membrane independent from Event 1 (Event 2). Supplementary Video S14 shows all 500 sections. Red arrows indicate paramural body-like structures (circular structures that appear to be fusing with the plasma membrane); V = vacuole.

cotyledons and leaves with trypan blue (Supplementary Fig. S3). These analyses revealed no cell death at 60 hpi for incompatible interactions in either leaves or cotyledons (Supplementary Fig. S3).

Although SBF-SEM imaging enabled us to identify a large number of putative PMBs, the xy resolution of SBF-SEM was insufficient to detect structures inside these putative PMBs. Therefore, we used a FIB-SEM imaging system, which has an xy resolution of approximately 3 nm to better visualize the same resin block shown in Supplementary Figure S1E, Figure 5, and Supplementary Video S14. SBF-SEM uses a microtome to slice thin sections (40-nm thickness) of the imaging surface parallel to the surface of the stub onto which the resin block is mounted, whereas FIB-SEM uses a gallium ion beam to mill thin layers of the imaging surface perpendicular to the stub surface. The resulting images are thus perpendicular to that produced by the SBF-SEM. Figure 6 and Supplementary Videos S15 and S16 show images obtained using a FIB-SEM. The cell wall, host cell plasma membrane, and the tonoplast membrane appear intact. Figure 6C captures the neck region in which an MVB appears to be fusing with the plasma membrane. We used IMOD to reconstruct and model this MVB and adjacent plant membranes (Supplementary Video S17). Figure 6E shows the modeled MVB (blue) above the cell wall (green) with the tonoplast membrane (pink) surrounding the MVB. Figure 6F shows the plasma membrane (white) instead of the tonoplast. Taken together, these images show us that the structures identified by SBF-SEM fusing to the plasma membranes are indeed derived from multivesicular endosomes, as they contain internal vesicles. Supplementary Videos S18 and S19 (enlarged S18) show another MVB with internal vesicles fusing with the plasma membrane. These structures are thus PMBs and are likely depositing vesicles and other defense-related compounds between the plasma membrane and cell wall.

Fungal infection induces secretion of EVs

The numerous PMBs induced during the incompatible interaction suggested that large numbers of EVs should be released. So, we quantified EV release during compatible (*C. destructivum*) and incompatible (*C. higginsianum*) interactions by collecting apoplastic wash fluid and assessing EV content at both 24 and 60 hpi (Fig. 7). We only counted particles between the size ranges of 50 to 250 nm, which is the typical size range of EVs, and plotted them in Figure 7A and C. At 24 hpi, we did not see a significant increase in vesicle secretion relative to mockinfected plants, even though we observed increased numbers of intracellular vesicles at this time point (Figs. 1 and 2).

By the 60-h time point, however, we observed a significant increase in EV secretion, with the greatest number of vesicles being secreted in the incompatible interaction, with about a three-fold increase in particle numbers relative to mock-infected plants (Fig. 7C). To confirm that we had indeed isolated vesicles, we performed negative stain TEM. Numerous cup-shaped objects (collapsed spheres) ranging in size between 50 and 250 nm in diameter were visible, which is typical of EVs. Very few other objects of this size were visible, indicating that the majority of the particles in this size range were EVs. We further confirmed this by performing immunoblots using an antibody to the EV marker protein PEN1 (Rutter and Innes 2017). Supplementary Figure S5 shows that PEN1 was present in p40 pellets isolated at both 24 and 60 hpi. The increase in EV numbers correlates with the abundance of MVBs and PMBs seen in incompatible interactions (Figs. 4A and B and 5; Supplementary Fig. S1E; Supplementary Videos S12 and S14). Notably, EV numbers observed in the compatible interaction were also higher than the mock at 60 hpi (Fig. 7C), suggesting that EVs may also be released via mechanisms that do not involve PMBs. Together, these results suggest that EVs are playing a role in the immune response during an incompatible interaction.

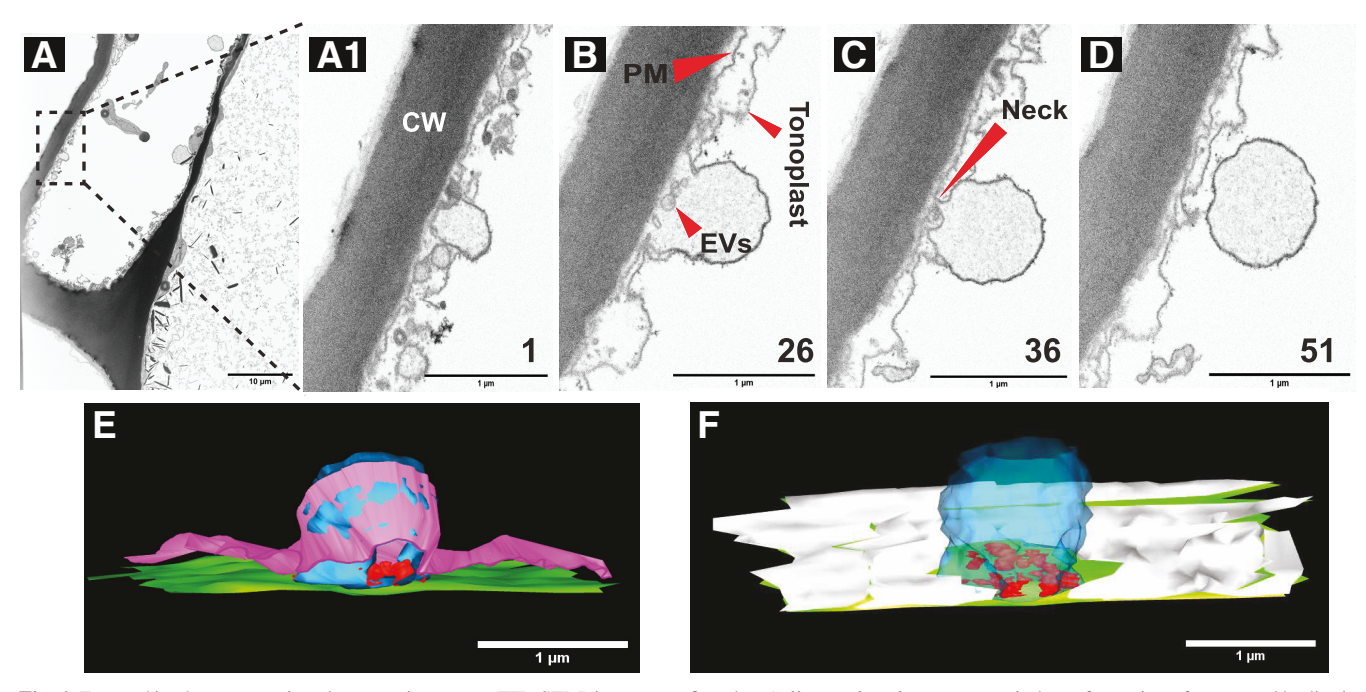


Fig. 6. Focused ion beam-scanning electron microscopy (FIB-SEM) images confirm that *Colletotrichum higginsianum* induces formation of paramural bodies in alfalfa epidermal cells. A, First micrograph from a stack of 51 images obtained using FIB-SEM. Supplementary Video S15 shows the entire stack. Supplementary Video S16 shows the stack with the paramural body region enlarged. The black box in A shows an area enlarged in panels A1 through D, which highlights a paramural body. A1, B, C, and D, The first, 26th, 36th, and 51st micrographs of the 51-image stack. Supplementary Video S16 shows all 51 images of this region. The plasma membrane (PM), tonoplast, and cell wall (CW) are all labeled. E and F, Three-dimensional models generated using IMOD of the region shown in panels A1 through D. Green represents the plant CW, red highlights the vesicular contents inside the paramural body, blue corresponds to the limiting membrane of the paramural body, pink indicates the tonoplast, and white indicates the PM in F. Supplementary Video S17 shows the model of the entire stack rotating in space.

Discussion

We compared the infection process between compatible and incompatible species of Colletotrichum on alfalfa by performing serial sections of the plant-fungal interface using SBF-SEM and FIB-SEM. We wanted to answer some key questions: how do these infection structures differ between a compatible and incompatible interaction at an ultrastructural level? Are there any structures unique to the incompatible interaction and vice versa? Can we see the origins of EVs that are released during plant-fungal interactions? The image stacks from these SEM images allowed us to generate 3D models of infection sites, which revealed multiple features that would have been missed using standard TEM. However, before detailing the features revealed by 3D modeling, we will first discuss the relative strengths and weaknesses of SBF-SEM and FIB-SEM as compared with standard TEM and light microscopy, along with limitations of the present study.

A strength of SBF-SEM relative to both FIB-SEM and standard TEM is the large sample area in three dimensions (individual sample volume) that can be imaged in a relatively short

time (e.g., 24 h of microscope time per sample). This enables imaging of multiple cells in a single imaging session in all three dimensions. However, this comes at a cost in terms of resolution. In our case, we were unable to resolve vesicles smaller than about 200 nm using SBF-SEM. We were unable to increase the magnification beyond that shown during our imaging sessions due to charge accumulation on sample blocks induced by the electron beam. Such charge accumulation is particularly problematic with leaf samples due to the large vacuoles in each cell. Vacuoles do not stain well with metal-based EM stains and thus do not conduct electrons well, which results in electron accumulation on the block face at higher magnifications and thus poor image quality. To overcome this problem, we employed FIB-SEM, which enables imaging at higher magnifications in all three dimensions compared with SBF-SEM. FIB-SEM also does not suffer from the charge accumulation issue observed with SBF-SEM. However, FIB-SEM is slower than SBF-SEM because each section must be removed by milling rather than with a microtome, and the total area that can be imaged in single image is much less. The increase in required microscope time typically means an increase in expense.

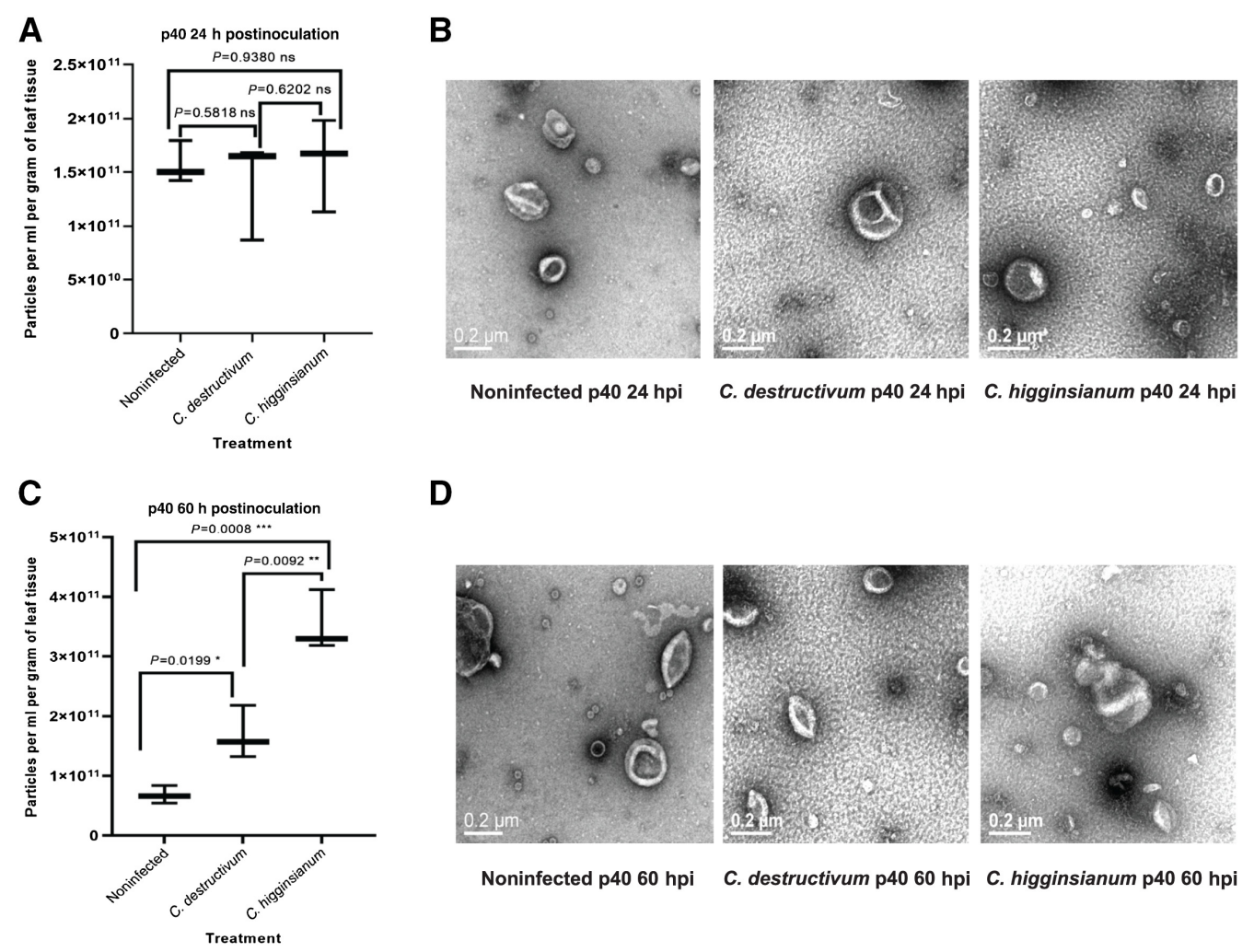


Fig. 7. Inoculation with an incompatible fungus induces extracellular vesicle (EV) release in alfalfa leaves. **A,** Quantification of EVs isolated from either mock-infected alfalfa leaves or alfalfa leaves infected with *Colletotrichum destructivum* (compatible) or *C. higginsianum* (incompatible) at 24 h postinoculation (hpi). EVs were isolated by ultracentrifugation of apoplastic wash fluid at $40,000 \times g$ (p40) and then quantified using a nanoparticle tracker. The counts of particles between the size range of 50 and 250 nm are plotted in the graph, indicating the true EV population. Data from three biological replicates for each treatment are shown. Error bars indicate standard deviation (SD). *P* values were calculated using a two-tailed unpaired Student's *t* test. **B,** Negative stain transmission electron microscopy (TEM) images of p40 fractions from representative replicates at 24 hpi. **C,** Quantification of EVs (particles between 50 and 250 nm) isolated at 60 hpi. **D,** Negative stain TEM images of p40 fractions from representative replicates at 60 hpi. ns = not significant; * P < 0.05; *** P < 0.01; *** P < 0.001.

Both SBF-SEM and FIB-SEM greatly facilitate 3D reconstructions compared with standard TEM because there is no need to collect and image serial sections that have been sliced off of a block, which can be very challenging, especially when collecting hundreds of sections as was done in the present study. Because each image from SBF-SEM and FIB-SEM is generated from a block face, it is also easier to align serial images compared with images of independent sections generated for standard TEM, which often have artifacts induced by uneven shrinkage or expansion of ultrathin sections. That said, TEM still offers the highest possible resolution and may be necessary when one needs to image structures smaller than 10 nm.

Although the above EM technologies offer outstanding resolution compared with light microscopy, especially of live cells, the present study is limited by the fact that we are imaging fixed, resin-embedded cells and are thus using static images to understand a dynamic process. This is particularly relevant to assessing whether vesicles that are fused to the plasma membrane are in the process of endocytosis or exocytosis. In this study, we have assumed that all such vesicles observed by SBF-SEM are in the process of exocytosis. This assumption is supported by several observations. First, higher resolution images obtained using FIB-SEM revealed the presence of EVs outside the plasma membrane immediately adjacent to these fusions. It is unlikely that such EVs would be present during endocytosis. Second, these presumptive PMBs are quite large, pushing into the vacuole against the turgor pressure of the vacuole. It is unclear how endocytosis could generate such a large invagination of the plasma membrane without anything pushing from the outside. Lastly, these PMBs were specifically induced by inoculation with an incompatible fungus, which we showed resulted in a large increase in vesicle secretion. It seems unlikely that, at the same time, the cells would be undergoing a large increase in a highly unusual form of endocytosis.

Although SBF-SEM is limited in resolution compared with standard TEM, we were still able to resolve extensive accumulation of circular structures along the periphery of inoculated cells induced by both compatible and incompatible Colletotrichum species. Most of the circular structures were electron-opaque, while some were lightly stained. In addition, the incompatible interaction also accumulated circular structures with no internal staining, which were not present in the compatible interaction at this time point. By using SBF-SEM, we were able to trace these circular structures through the volume of the plant cell to see if they were vesicular or tubular in 3D imaging. This work revealed that many were, in fact, tubular and were interconnected, forming a mesh-like network. Previous studies that employed standard TEM to image fungal infection sites on plant cells have revealed similar circular structures, which were assumed to be spherical vesicles or organelles (O'Connell 1987; O'Connell et al. 1985; Politis 1976; Wharton et al. 2001), but from our SBF-SEM observations, we now expect these may have been cross-sections through more complex structures. Regardless, the accumulation of vesicles and tubules along the periphery of inoculated cells appears to be an immune response, as they were not seen in noninfected control leaves.

By 24 hpi, both compatible and incompatible *Colletorichum* species had formed appressoria, while neither fungal species had penetrated the host cell wall. This is consistent with previous reports of compatible interactions between cucumber leaves and *C. lagenarium* (Xuei et al. 1988), maize leaves and *C. graminicola* (Mims and Vaillancourt 2002), and bean leaves and *C. lindemuthianum* (O'Connell et al. 1985).

At 60 hpi with the compatible pathogen, we observed penetration pegs beneath appressoria that gave rise to bulbous biotrophic hyphae. These hyphae displaced the majority of the plant cell central vacuole; 3D modelling enabled us to see the large vol-

ume occupied by these hyphae and their branching. This would not be posible with standard TEM. This finding is consistent with TEM-based observations of *C. lindemuthianum* infecting epidermal cells of French bean, which showed cross-sections of large biotrophic hyphae displacing epidermal cell central vacuoles at 4 days postinoculation (O'Connell et al. 1985). Similar bulbous biotrophic hyphae that arise from appressoria have also been observed with *C. sublineola* infecting sorghum epidermal cells (Wharton et al. 2001) and in multiple other compatible *Colletotrichum*-plant interactions using both light and EM, including the *C. gloeosporioides*—tangerine interaction (Brown 1977), *C. graminicola*—maize interaction (Mims and Vaillancourt 2002), and *C. lagenarium* (now called *C. orbiculare*)—cucumber interaction (Xuei et al. 1988).

In contrast to the compatible interaction, we did not observe any penetration pegs or biotrophic hyphae in the incompatible interaction at 60 hpi. This observation is similar to that observed in Arabidopsis infected with incompatible (nonadapted) Colletotrichum species (Shimada et al. 2006), which indicates that incompatible fungi are typically stopped prior to penetration of the host cell wall without induction of host cell death. This differs from resistant interactions to compatible (adapted) species of fungi, which typically are induced following penetration of the host cell and secretion of effectors (Irieda et al. 2014; Kleemann et al. 2012). For example, small intracellular hyphae with no interfacial matrix were observed in resistant bean varieties infected with C. lindemuthianum (O'Connell et al. 1985). Similarly, formation of penetration pegs with occasional biotrophic hyphae have been observed in resistant sorghum infected with C. sublineola (Wharton et al. 2001), resistant oats infected with C. graminicola (Politis 1976), and resistant cucumber infected with C. lagenarium (Xuei et al. 1988).

Although we did not observe host cell death or penetration of the host cell wall during incompatible interactions, extensive production of electron-opaque vesicle-like structures was seen, mostly beneath appressoria; 3D modelling revealed these structures to be compact layers of interconnected membranes. This meshwork is likely part of a local accumulation of host cytoplasm associated with papilla formation. Papilla formation occurs in response to several Colletotrichum species during both host and nonhost interactions. For example, papilla formation was observed in resistant and susceptible M. sativa infected with C. trifolii (Mould and Robb 1992; Mould et al. 1991); cucumber plants infected with virulent or avirulent C. lagenarium strains (Xuei et al. 1988); sorghum infected with virulent or avirulent C. sublineola (Wharton et al. 2001); French bean infected with virulent or avirulent C. lindemuthianum (O'Connell et al. 1985); Arabidopsis infected with a nonhost Colletotrichum species (Shimada et al. 2006); and oats infected with avirulent C. graminicola (Politis 1976). Although papillae fail to stop infection of virulent Colletotrichum strains, it is thought that they contribute to resistance against avirulent and nonhost strains. This is based, in part, on differences in the appearance of papillae formed during resistant and nonhost interactions versus those formed during susceptible interactions. For example, resistant sorghum produces papillae that are more electron-opaque compared with those formed by a susceptible variety, and papillae in the resistant variety are penetrated at a lower rate compared with those of the susceptible variety (Wharton et al. 2001). Similarly, penetration of papillae formed in cucumber occurs at a much lower frequency during infection by avirulent strains than during infection by virulent strains (Xuei et al. 1988).

In addition to revealing the complex membrane arrangements present in the papilla precursors or cytoplasmic aggregates, our 3D EM analyses revealed a dramatic increase in plant PMB formation during the incompatible interaction with *C. higginsianum* compared with the compatible interaction with *C. destructivum*.

To our knowledge, this is the first report of plant PMBs accumulating in response to challenge by a nonadapted or incompatible fungal pathogen, and the finding suggests that PMBs could contribute to the *Medicago* defense response.

PMBs are thought to be formed by the fusion of MVBs with the plasma membrane, thereby depositing the vesicles, and any other components found inside the limiting membrane of the MVB, outside the plasma membrane. PMBs have been observed previously near the vicinity of papillae during both compatible and incompatible interactions with both hemibiotrophic *Colletotrichum* as well as with the biotrophic powdery mildew fungus *Blumeria graminis* f. sp. *hordei* (An et al. 2006a, b). Our SBF-SEM data revealed, however, that PMBs were broadly distributed around the periphery of the cell and were not limited to the region around papillae.

The increase in PMB formation during the incompatible interaction suggested that there should be an increase in EV release. Therefore, we isolated EVs from both compatible and incompatible interactions at both 24- and 60-h time points. These analyses revealed that, compared with mock-infected plants, EV abundance increased more than three-fold by 60 hpi with the incompatible strain and approximately two-fold with the compatible strain. The increase observed with the compatible strain in the absence of an obvious increase in PMBs suggests that plants may also release EVs using a mechanism independent of PMBs. The increase in EV abundance with both compatible and incompatible strains is consistent with our previous findings that plants sprayed with salicylic acid or infected with *Pseudomonas syringae* increase EV abundance approximately two-fold (Rutter and Innes 2017).

Taken together, our results suggest that PMBs and papillae contribute to nonhost resistance in plants and that the contents of PMBs, including EVs, may play a role in such resistance. Further study is required to investigate the contents of the EVs released during incompatible interactions and how these differ from EVs isolated from uninfected plants.

Materials and Methods

Fungal material

C. destructivum isolate CBS 520.97 (https://wi.knaw.nl/ Collection) and C. higginsianum isolate IMI349063A were used for infections. The fungal stocks were stored at -80° C in $1\times$ potato dextrose broth supplemented with 20% glycerol. Fungal cultures were prepared by spotting cultures from glycerol stocks onto solid Mathur's Media (2.8 g/liter of glucose, 2.2 g/liter of mycological peptone, 0.5 g/liter of yeast extract, 1.2 g/liter of MgSO₄·7H₂O, 2.7 g/liter of KH₂PO₄, and 20 g/liter of agar, with a pH of 5.5). Plates were kept in the dark for 24 h and then allowed to grow for 3 weeks under short day photoperiod conditions (9-h days, 22°C, and 150 μEm⁻²s⁻¹). For harvesting the spores, 1 ml of sterile deionized water was applied to the Mathur's plate, and the spores were dislodged using a sterilized glass rod. The spore solution was transferred to a microfuge tube, and the spores were pelleted at $2,000 \times g$ for 5 min, discarding the supernatant containing the mycelia. The spore pellet was washed five times with 1 ml of deionized water, centrifuging each time at $2,000 \times$ g for 5 min. The final pellet was resuspended in sterile deionized water, and spores were counted using a Neubauer chamber and adjusted to the desired concentration.

Plant material and growth conditions for spot inoculation and vesicle isolation

Alfalfa (*M. sativa*) seeds were sterilized using 10% bleach (30 s) and 70% ethanol (2 min) followed by five rinses in sterile deionized water. The sterilized seeds were placed on Pro-Mix PGX potting mix inside a humidity chamber that was created by

placing pots inside a plastic box which in turn was placed inside a plastic bag. The seeds were stratified at $4^{\circ}C$ for 24 h before moving them to a growth room (10-h days, $24^{\circ}C$, and $150\,\mu\text{Em}^{-2}\text{s}^{-1})$ for 7 days. Each cotyledon was spot inoculated with approximately 5 μ l of 2×10^6 spores/ml (mixed with 0.001% Silwet) of either *C. higginsianum* (incompatible) or *C. destructivum* (compatible) spores. Inoculated plants were incubated in the dark for 12 h at 100% humidity at 25°C before being transferred to the short-day room. For mock-inoculated controls, approximately 5 μ l of sterile deionized water (mixed with 0.001% Silwet) was spotted onto each cotyledon under identical conditions as the infected samples. The water droplet or the fungal droplet did not evaporate even after 60 h, suggesting that the humidity chamber maintained 100% humidity.

For vesicle isolation, alfalfa seeds were sterilized and stratified as described above and were then grown in a growth room as described above for 3 weeks before being sprayed with either $C.\ higginsianum$ or $C.\ destructivum$ spores (2 × 10⁶ spores/ml mixed with 0.001% Silwet) or water (mixed with 0.001% Silwet) as a control. The sprayed plants were covered with a plastic dome and placed inside plastic bags to maintain humid conditions until vesicle isolation at either 24 or 60 hpi.

Sample fixation, staining, and resin embedding

Inoculated regions of alfalfa cotyledons were sampled using a 2-mm biopsy punch at either 24 or 60 hpi. Several 2-mm discs were collected for each infection condition, and the discs were placed in an 8-ml glass sample vial with a rubber-lined cap (Wheaton, Catalog #224884) and vacuum infiltrated with fixative solution composed of 4% glutaraldehyde (v/v, EM Grade, Electron Microscopy Sciences [EMS], Catalog #16020) and 4% formaldehyde (v/v, EM Grade, EMS, Catalog #15710) in 100 mM sodium phosphate (SP) buffer with a pH of 7.2 until the samples sank to the bottom. Infiltrated samples were incubated at 4°C under constant rotation for 24 to 36 h. The sample was washed five times for 10 min each with SP buffer and was then transferred to a freshly prepared solution containing 1.5% potassium ferrocyanide (w/v, SIGMA Life Science, Lot #BCBV7953) and 2% OsO₄ (v/v, EM Grade, EMS, Catalog #19150) solution in SP buffer for 2 h at room temperature while rotating. Subsequently, the samples were washed five times for 10 min each with sterile deionized water, transferred to fresh solution containing 1% (w/v) thiocarbohydrazide (EMS, Catalog #21900) in deionized water, and incubated for 1 h under rotation at room temperature. The samples were then washed with deionized water five times for 10 min and incubated with 2% OsO₄ (v/v) in deionized water for 2 h at room temperature. The samples were again washed with deionized water five times for 10 min before staining with 0.2% (w/v) uranyl acetate (EMS, Catalog #22400) in water overnight at 4°C. The samples were again washed five times with deionized water for 10 min each before being gradually dehydrated with 10 (v/v), 25, 50, 75, and $3 \times 100\%$ acetone for 30 min each. Samples were infiltrated with Durcupan resin (EMS, Catalog #14040) in 10 (v/v in acetone), 25, 50, 75, and 5 × 100% resin over a period of 3 days. Samples were carefully layered on top of fresh resin during each of the 100% resin infiltration steps and centrifuged at $376 \times g$ until the samples reached the bottom of the 2-ml centrifuge tubes (usually approximately 2 min) (McDonald 2014). Samples were finally flatembedded in Durcupan using Aclar (Kingsley and Cole 1988) or flat-embedding molds in an oven at 60°C.

Sample preparation for EM

Samples embedded in resin were first trimmed roughly using a jeweler's saw and then mounted on aluminum stubs using EPO-TEK electrically conductive resin, which was allowed to solidify in an oven at 60°C overnight. Samples were trimmed by

hand using a double-edged razor blade to an approximate height of 0.5 mm, a length of 2 mm, and a width of 300 μm , followed by sputter-coating with 45 nm 80:20 Au:Pd at 3.8 $\times~10^{-2}$ Torr and 30 mA using the Safematic Compact Coating Unit (CCU)-010 before smoothing the block face with a diamond knife (Diatome) using a Leica Ultracut ultramicrotome.

SBF-SEM

Samples were imaged using a Thermo Fisher Teneo Volume Scope equipped with an in situ ultramicrotome, which was set to remove 40- μ m sections with each slice. Images of the block face were obtained at 2.5 kV/0.8 nA at a low vacuum pressure of 50 pa with the VS-DBS detector for backscatter. Each of the images were 6,144 \times 4,096 pixels with an xy pixel size of 10 nm. The images obtained were first-batch inverted using Adobe Photoshop CC and processed using IMOD (Kremer et al. 1996). This software was used to perform segmentation and 3D reconstructions. Videos were created from serial images using the Windows 10 Media player function.

FIB-SEM

FIB-SEM image acquisition was performed using a Zeiss Auriga 60 FIB-SEM with ATLAS 3D software (FIBICs, Carl Zeiss Microscopy). We used a sample preparation workflow containing the following steps: (i) deposit a 30- \times 20- μ m platinum pad of 1-µm thickness on the sample surface over the region of interest using the gas injection system (GIS); (ii) mill tracking and autotune marks in the platinum pad using the gallium ion beam; (iii) deposit a carbon layer of 1-µm thickness onto the tracking and autotune marks for protection during the milling and imaging process; (iv) coarse trench mill (30-µm width and 30-µm depth); and (v) trench polish (30-µm width and 30-µm depth). The SEM images were acquired at 1.5 kV with the energy-selective backscattered electron (EsB) detector at a grid voltage of 750 V and 1 nA of electron beam current (60-um aperture and high current mode). The pixel dwell time was 1 us with a line average of 1. The xy pixel size was 3 nm, and the slicing thickness in the z direction was 12 nm. During the milling and imaging process, the FIB was operated at continuous milling mode at 30 kV and 600 pA of ion beam current with a milling rate of 8 nm/min. About 700 images were acquired continuously in a period of about 19 h.

Vesicle isolation

Apoplastic wash fluid was isolated from 3-week-old alfalfa plants following the protocol described in Rutter and Innes (2017). In brief, leaves were vacuum infiltrated with vesicle isolation buffer (VIB, 20 mM MES, 2 mM CaCl₂, and 0.1 M NaCl, with a pH of 6). The excess buffer was removed from the surface of the leaves using Kimwipes. The leaves were placed inside needleless 30-ml syringes (making sure not to overstuff the syringes), and the syringes were placed inside 50-ml screwcap tubes. The tubes were centrifuged for 20 min at $700 \times g$ with slow acceleration at 4°C using a JA-14 rotor (Avanti J-20 XP centrifuge; Beckman Coulter). The resulting apoplastic wash collected was passed through a 0.22-um membrane filter to remove bacteria and larger debris. The supernatant was transferred to new 13- \times 51-mm polycarbonate centrifuge tubes (Beckman Coulter #349622) and centrifuged at $10,000 \times g$ for 30 min at 4°C using a TLA100.3 fixed-angle rotor and an Optima TLX Ultracentrifuge (Beckman Coulter). Supernatants were transferred to new centrifuge tubes and centrifuged at $40,000 \times g$ for 1 h at 4°C using the same rotor. The resulting pellet was washed using VIB and repelleted at $40,000 \times g$ for 1 h at 4°C. The final pellet was resuspended in 50 µl of fresh filtered VIB and kept on ice for further experiments or stored at -80° C for subsequent use.

Nanoparticle tracking analysis

Particle concentrations and diameters were determined using a ZetaView Particle Tracking Analyzer (Particle Metrix, Diessen) and its built-in software. The analyzer was first calibrated using 100-nm polystyrene beads. Vesicle samples were diluted 1:1,000 times using fresh VIB with a pH of 6.0. The ZetaView was operated with a max diameter setting of 500 nm and minimum diameter setting of 5 nm. For data analysis, the percentage of particles that were between 50 to 250 nm in diameter was calculated and plotted in the graph.

TEM of EVs

Aliquots (5 μ l) of resuspended p40 pellets were spotted onto Formvar and carbon-coated copper EM grids (EMS) that were glow-discharged at 15 mA for 60 s prior to application of samples. After 5 min, the excess sample was wicked off using filter paper. Following that, 10 μ l of 2% uranyl acetate was applied to the grids for 2 min. The excess solution was wicked off using filter paper, and the grids were allowed to air-dry overnight. The grids were imaged using a JEM-1010 transmission electron microscope (JEOL, U.S.A.) at 80 kV.

Trypan blue staining

Alfalfa cotyledons and leaves were first stripped of their chlorophyll by incubating in 1:3 w/v solution of acetic acid:95% ethanol overnight with gentle shaking. For staining, a stock solution of trypan blue (10 g of phenol, 10 ml of lactic acid, 10 ml of glycerol, 10 ml of deionized water, and 0.02 g of trypan blue [Sigma-Aldrich 302643-25G]) was diluted with 95% ethanol (1:2 v/v). Samples were placed in a 55°C water bath with 1 ml of trypan blue solution for 1 min and were transferred to a 4°C water bath overnight with gentle shaking. To destain, chloral hydrate solution was prepared by mixing 1,000 g of chloral hydrate (Sigma-Aldrich 302-17-0) in 400 ml of deionized water (which takes several hours to dissolve). Samples were incubated in chloral hydrate solution for a minimum of 3 h, with replacement of the solution approximately once per hour.

Aniline blue staining

Alfalfa cotyledons and leaves were first stripped of their chlorophyll by placing them in 1:3 w/v solution of acetic acid:95% ethanol overnight with gentle shaking. The samples were subsequently rehydrated with 150 mM phosphate buffer with a pH of 8.0 for 30 min. Samples were stained in 150 mM phosphate buffer with a pH of 8.0 containing 0.01% (w/v) aniline blue (Sigma-Aldrich 28631-66-5) at 4°C overnight. Samples were imaged using a Nikon NiE microscope equipped with a DAPI filter.

Immunoblots

For immunoblot analysis, p40 pellets were resuspended in 50 µl of VIB buffer, and 20 µl of this suspension was mixed with 5 µl of $5\times$ SDS loading buffer (8% SDS, 250 mM Tris-HCl with a pH of 6.8, 0.1% Bromophenol Blue, 40% glycerol, and 400 mM dithiothreitol) and heated at 95°C for 5 min. Cell lysates (positive controls) were prepared by freezing 500 mg of leaf tissue in liquid nitrogen and grinding with a mortar and pestle. Ground leaf tissue was extracted in 1 ml of protein extraction buffer (50 mM Tris-HCl with a pH of 7.0, 150 mM NaCl, 0.1% Nonidet P-40, 1% plant protease inhibitor cocktail [Sigma-Aldrich], and 1% 2,2′-dipyridyldisulfide) and centrifuged at 12,500 × g for 10 min at 4°C to pellet debris; 20 µl of supernatant was then mixed with 5 µl of $5\times$ SDS loading buffer and heated at 95°C for 5 min.

Samples were loaded on 4 to 20% Precise Protein Gels (Thermo Scientific) and electrophoresed at 120V for 1 h in Tris-SDS running buffer (30.0 g of Tris base, 144.0 g of glycine,

and 10.0 g of SDS in 1,000 ml of H_2O with a pH of 8.3 $[10\times]$ diluted to $1\times$ before use). The proteins were transferred to a nitrocellulose membrane (Amersham Protran Premium 0.45- μ m NC product 10600003). Ponceau staining was used to confirm successful transfer and equal loading of samples. Membranes were washed with Tris-buffered saline (50 mM Tris-Cl and 150 mM NaCl with a pH of 7.5) containing 0.1% Tween 20 (TBST) and blocked with 5% Difco Skim Milk (BD) overnight at 4°C. Membranes were incubated with anti-PEN1 antibody (Zhang et al. 2007) at a 1:1,000 dilution for 1 h, washed with TBST, and incubated with horseradish peroxidase-labeled goat anti-rabbit antibody (Abcam AB97051) at a 1:5,000 dilution for 1 h. After a final wash in TBST, protein bands were imaged using a BIO-RAD ChemiDoc Imaging system.

Acknowledgments

We thank the Indiana University (IU) Bloomington Electron Microscopy Center for access to a Leica Ultracut ultramicrotome, JEOL JEM 1010 Transmission Electron Microscope, and Thermo Fisher Teneo VolumeScope. We also thank the IU Bloomington Nanocharacterization Facility (NCF) for access to a Zeiss Auriga 60 FIB-SEM and to NCF/IUB-EMC staff member Jun Chen for assistance with this equipment.

Author-Recommended Internet Resource

IMOD home page: https://bio3d.colorado.edu/imod/

Literature Cited

- An, Q., Ehlers, K., Kogel, K.-H., Van Bel, A. J. E., and Hückelhoven, R. 2006a. Multivesicular compartments proliferate in susceptible and resistant *MLA12*-barley leaves in response to infection by the biotrophic powdery mildew fungus. New Phytol. 172:563-576.
- An, Q., Hückelhoven, R., Kogel, K.-H., and Van Bel, A. J. E. 2006b. Multivesicular bodies participate in a cell wall-associated defence response in barley leaves attacked by the pathogenic powdery mildew fungus. Cell. Microbiol. 8:1009-1019.
- Assaad, F. F., Qiu, J.-L., Youngs, H., Ehrhardt, D., Zimmerli, L., Kalde, M., Wanner, G., Peck, S. C., Edwards, H., Ramonell, K., Somerville, C. R., and Thordal-Christensen, H. 2004. The PEN1 syntaxin defines a novel cellular compartment upon fungal attack and is required for the timely assembly of papillae. Mol. Biol. Cell 15:5118-5129.
- Bhunjun, C. S., Phukhamsakda, C., Jayawardena, R. S., Jeewon, R., Promputtha, I., and Hyde, K. D. 2021. Investigating species boundaries in *Colletotrichum*. Fungal Divers. 107:107-127.
- Böhlenius, H., Mørch, S. M., Godfrey, D., Nielsen, M. E., and Thordal-Christensen, H. 2010. The multivesicular body-localized GTPase ARFA1b/1c is important for callose deposition and ROR2 syntaxin-dependent preinvasive basal defense in barley. Plant Cell 22: 3831-3844.
- Brown, G. E. 1977. Ultrastructure of penetration of ethylene-degreened Robinson tangerines by *Colletotrichum gloeosporioides*. Phytopathology 67:315-320
- Buono, R. A., Paez-Valencia, J., Miller, N. D., Goodman, K., Spitzer, C., Spalding, E. P., and Otegui, M. S. 2016. Role of SKD1 Regulators LIP5 and IST1-LIKE1 in endosomal sorting and plant development. Plant Physiol. 171:251-264.
- Crous, P. W., Gams, W., Stalpers, J. A., Robert, V., and Stegehuis, G. 2004. MycoBank: An online initiative to launch mycology into the 21st century. Stud. Mycol. 50:19-22. https://www.mycobank.org/
- Damm, U., O'Connell, R. J., Groenewald, J. Z., and Crous, P. W. 2014. The *Colletotrichum destructivum* species complex - hemibiotrophic pathogens of forage and field crops. Stud. Mycol. 79:49-84.
- da Silva, L. L., Moreno, H. L. A., Correia, H. L. N., Santana, M. F., and de Queiroz, M. V. 2020. *Colletotrichum*: Species complexes, lifestyle, and peculiarities of some sources of genetic variability. Appl. Microbiol. Biotechnol. 104:1891-1904.
- Denk, W., and Horstmann, H. 2004. Serial block-face scanning electron microscopy to reconstruct three-dimensional tissue nanostructure. PLoS Biol. 2:e329.
- Ellinger, D., Naumann, M., Falter, C., Zwikowics, C., Jamrow, T., Manisseri, C., Somerville, S. C., and Voigt, C. A. 2013. Elevated early callose deposition results in complete penetration resistance to powdery mildew in Arabidopsis. Plant Physiol. 161:1433-1444.

- Fernández-Bautista, N., Domínguez-Núñez, J. A., Moreno, M. M. C., and Berrocal-Lobo, M. 2016. Plant tissue trypan blue staining during phytopathogen infection. Bio-Protocol 6:e2078.
- Heath, M. C. 2000. Nonhost resistance and nonspecific plant defenses. Curr. Opin. Plant Biol. 3:315-319.
- Heitefuss, R., and Ebrahim-Nesbat, F. 1986. Ultrastructural and histochemical studies on mildew of barley (*Erysiphe graminis* DC. f. sp. hordei Marchal). J. Phytopathol. 116:358-373.
- Irieda, H., Maeda, H., Akiyama, K., Hagiwara, A., Saitoh, H., Uemura, A., Terauchi, R., and Takano, Y. 2014. *Colletotrichum orbiculare* secretes virulence effectors to a biotrophic interface at the primary hyphal neck via exocytosis coupled with SEC22-mediated traffic. Plant Cell 26:2265-2281
- Jacobs, A. K., Lipka, V., Burton, R. A., Panstruga, R., Strizhov, N., Schulze-Lefert, P., and Fincher, G. B. 2003. An Arabidopsis callose synthase, GSL5, is required for wound and papillary callose formation. Plant Cell 15:2503-2513.
- Kingsley, R. E., and Cole, N. L. 1988. Preparation of cultured mammalian cells for transmission and scanning electron microscopy using Aclar film. J. Electron Microsc. Tech. 10:77-85.
- Kleemann, J., Rincon-Rivera, L. J., Takahara, H., Neumann, U., Ver Loren van Themaat, E., van der Does, H. C., Hacquard, S., Stüber, K., Will, I., Schmalenbach, W., Schmelzer, E., and O'Connell, R. J. 2012. Sequential delivery of host-induced virulence effectors by appressoria and intracellular hyphae of the phytopathogen *Colletotrichum higginsianum*. PLoS Pathog. 8:e1002643.
- Kremer, J. R., Mastronarde, D. N., and McIntosh, J. R. 1996. Computer visualization of three-dimensional image data using IMOD. J. Struct. Biol. 116:71-76.
- Latunde-Dada, A. O., Bailey, J. A., and Lucas, J. A. 1997. Infection process of *Colletotrichum destructivum* O'Gara from lucerne (*Medicago sativa* L.). Eur. J. Plant Pathol. 103:35-41.
- Liu, F., Ma, Z. Y., Hou, L. W., Diao, Y. Z., Wu, W. P., Damm, U., Song, S., and Cai, L. 2022. Updating species diversity of *Colletotrichum*, with a phylogenomic overview. Stud. Mycol. 101:1-56.
- Luna, E., Pastor, V., Robert, J., Flors, V., Mauch-Mani, B., and Ton, J. 2011.
 Callose deposition: A multifaceted plant defense response. Mol. Plant-Microbe Interact. 24:183-193.
- Luttrell, E. S. 1974. Parasitism of fungi on vascular plants. Mycologia 66:1-15.
- Marchant, R., and Robards, A. W. 1968. Membrane systems associated with the plasmalemma of plant cells. Ann. Bot. 32:457-471.
- McDonald, K. L. 2014. Rapid embedding methods into epoxy and LR White resins for morphological and immunological analysis of cryofixed biological specimens. Microsc. Microanal. 20:152-163.
- Mims, C. W., and Vaillancourt, L. J. 2002. Ultrastructural characterization of infection and colonization of maize leaves by *Colletotrichum graminicola*, and by a *C. graminicola* pathogenicity mutant. Phytopathology 92:803-812
- Mould, M. J. R., Boland, G. J., and Robb, J. 1991. Ultrastructure of the Colletotrichum trifolii-Medicago sativa pathosystem. I. Pre-penetration events. Physiol. Mol. Plant Pathol. 38:179-194.
- Mould, M. J. R., and Robb, J. 1992. The Colletotrichum trifolii Medicago sativa interface, in culture: A cytological analysis. Can. J. Bot. 70:114-124.
- O'Connell, R. J. 1987. Absence of a specialized interface between intracellular hyphae of *Colletotrichum lindemuthianum* and cells of *Phaseolus vulgaris*. New Phytol. 107:725-734.
- O'Connell, R. J., Bailey, J. A., and Richmond, D. V. 1985. Cytology and physiology of infection of *Phaseolus vulgaris* by *Colletotrichum linde-muthianum*. Physiol. Plant Pathol. 27:75-98.
- O'Connell, R., Herbert, C., Sreenivasaprasad, S., Khatib, M., Esquerré-Tugayé, M.-T., and Dumas, B. 2004. A novel *Arabidopsis-Colletotrichum* pathosystem for the molecular dissection of plant-fungal interactions. Mol. Plant-Microbe Interact. 17:272-282.
- O'Connell, R. J., Thon, M. R., Hacquard, S., Amyotte, S. G., Kleemann, J., Torres, M. F., Damm, U., Buiate, E. A., Epstein, L., Alkan, N., Altmüller, J., Alvarado-Balderrama, L., Bauser, C. A., Becker, C., Birren, B. W., Chen, Z., Choi, J., Crouch, J. A., Duvick, J. P., Farman, M. A., Gan, P., Heiman, D., Henrissat, B., Howard, R. J., Kabbage, M., Koch, C., Kracher, B., Kubo, Y., Law, A. D., Lebrun, M.-H., Lee, Y.-H., Miyara, I., Moore, N., Neumann, U., Nordström, K., Panaccione, D. G., Panstruga, R., Place, M., Proctor, R. H., et al. 2012. Lifestyle transitions in plant pathogenic *Colletotrichum* fungi deciphered by genome and transcriptome analyses. Nat. Genet. 44:1060-1065.
- Politis, D. J. 1976. Ultrastructure of penetration by *Colletotrichum graminicola* of highly resistant oat leaves. Physiol. Plant Pathol. 8: 117-122.

- Politis, D. J., and Wheeler, H. 1973. Ultrastructural study of penetration of maize leaves by *Colletotrichum graminicola*. Physiol. Plant Pathol. 3:465-471
- Regmi, K. C., Ghosh, S., Koch, B., Neumann, U., Stein, B., O'Connell, R. J., and Innes, R. W. 2024. Three-dimensional ultrastructure of *Arabidopsis* cotyledons infected with *Colletotrichum higginsianum*. Mol. Plant-Microbe Interact. 37:396-406.
- Rubiato, H. M., Liu, M., O'Connell, R. J., and Nielsen, M. E. 2022. Plant SYP12 syntaxins mediate an evolutionarily conserved general immunity to filamentous pathogens. eLife 11:e73487.
- Rutter, B. D., and Innes, R. W. 2017. Extracellular vesicles isolated from the leaf apoplast carry stress-response proteins. Plant Physiol. 173:728-741.
- Schmelzer, E. 2002. Cell polarization, a crucial process in fungal defence. Trends Plant Sci. 7:411-415.
- Shimada, C., Lipka, V., O'Connell, R., Okuno, T., Schulze-Lefert, P., and Takano, Y. 2006. Nonhost resistance in *Arabidopsis-Colletotrichum* interactions acts at the cell periphery and requires actin filament function. Mol. Plant-Microbe Interact. 19:270-279.
- Weir, B. S., Johnston, P. R., and Damm, U. 2012. The *Colletotrichum gloeosporioides* species complex. Stud. Mycol. 73:115-180.
- Wharton, P. S., Julian, A. M., and O'Connell, R. J. 2001. Ultrastructure of the infection of *Sorghum bicolor* by *Colletotrichum sublineolum*. Phytopathology 91:149-158.

- Xu, C. S., Hayworth, K. J., Lu, Z., Grob, P., Hassan, A. M., García-Cerdán, J. G., Niyogi, K. K., Nogales, E., Weinberg, R. J., and Hess, H. F. 2017. Enhanced FIB-SEM systems for large-volume 3D imaging. eLife 6: e25916
- Xu, H., and Mendgen, K. 1994. Endocytosis of 1,3-β-glucans by broad bean cells at the penetration site of the cowpea rust fungus (haploid stage). Planta 195:282-290.
- Xuei, X. L., Järlfors, U., and Kuć, J. 1988. Ultrastructural changes associated with induced systemic resistance of cucumber to disease: Host response and development of *Colletotrichum lagenarium* in systemically protected leaves. Can. J. Bot. 66:1028-1038.
- Yan, Y., Yuan, Q., Tang, J., Huang, J., Hsiang, T., Wei, Y., and Zheng, L. 2018. *Colletotrichum higginsianum* as a model for understanding host-pathogen interactions: A review. Int. J. Mol. Sci. 19: 2142
- Zeyen, R. J., and Bushnel, W. R. 1979. Papilla response of barley epidermal cells caused by *Erysiphe graminis*: Rate and method of deposition determined by microcinematography and transmission electron microscopy. Can. J. Bot. 57:898-913.
- Zhang, Z., Feechan, A., Pedersen, C., Newman, M.-A., Qiu, J.-I., Olesen, K. L., and Thordal-Christensen, H. 2007. A SNARE-protein has opposing functions in penetration resistance and defence signalling pathways. Plant J. 49:302-312.